

DESIGN OF A HIGH CHARGE CW PHOTOCATHODE INJECTOR TEST STAND AT CEBAF

H. Liu, D. Kehne, S. Benson, J. Bisognano, L. Cardman, F. Dylla, D. Engwall, J. Fugitt, K. Jordan, G. Neil, D. Neuffer, C. Sinclair, M. Wiseman and B. Yunn

CEBAF, 12000 Jefferson Avenue, Newport News, VA 23606, USA

A 10 MeV high-charge CW electron injector test stand has been designed for the CEBAF UV FEL driver accelerator. It consists of a 500 kV DC photocathode gun, a 1500 MHz room-temperature buncher, a modified CEBAF cryounit (quarter cryomodule) with an SRF accelerating gradient of ~ 10 MV/m, two solenoids in the 500 kV region and an achromatic, non-isochronous injection transport line delivering 10 MeV beam to the driver accelerator. Experimental work is in progress toward establishing design system performance.

I. INTRODUCTION

Based on a 500 kV DC laser gun [1] and the 1500 MHz SRF technologies established at CEBAF, a 10 MeV CW high charge electron injector has been designed and is being built for a recirculating, 200 MeV SRF accelerator [2] which will drive kW-level industrial UV/IR FELs [3]. The design approach we have adopted is shown schematically in Fig. 1. It is composed of a DC laser gun, a 1500 MHz room-temperature buncher, two solenoids, a cryounit containing two CEBAF SRF cavities, and an injection line consisting of a "zoom" lens (4 quads) and a 3-magnet achromatic, non-isochronous bending system. The injection line design is discussed elsewhere [4].

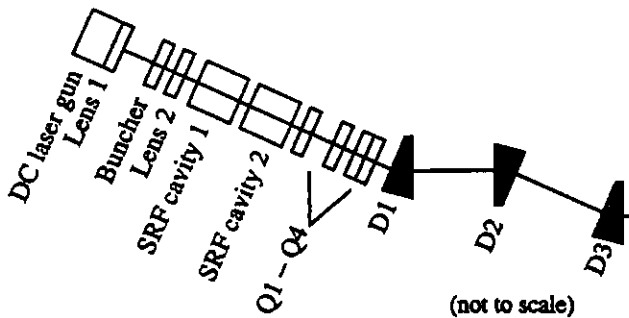


Fig. 1 Block diagram of the CEBAF FEL injector.

The design goal is to achieve the smallest practical transverse and longitudinal beam emittances at the end of the injector with a 135 pC charge/bunch. Electrons originate from a GaAs photocathode illuminated by a train of 60 ps (4σ) laser pulses. The design was carried out through extensive space-charge-dominated beam dynamics calculations consistently from the cathode to the entrance of the accelerator using a point-by-point space charge algorithm [5]. The modeling results show that this injector should be an excellent high-brightness source for an FEL, and that the requirements listed in Table 1 may be met. The details of the system components and performance modeling will be presented in the following sec-

tions.

Table 1 Requirements on the CEBAF FEL injector

Beam parameters	Requirements
Momentum (p)	10 MeV/c
Charge/bunch (Q)	135 pC
Repetition rate (f_p)	37.43 MHz
Average current (I)	5 mA
Tran. norm. emittance (ϵ_{nrms})	8π mm mrad
Longitudinal emittance ($\epsilon_{\phi rms}$)	20π keV-deg
Bunch length (σ_p)	1.5 ps
Matching conditions ($\beta_x/\beta_y, \alpha_x/\alpha_y$)	30/30 m, 0/0

II. HARDWARE COMPONENTS

The performance of the 500 kV photoemission gun is the most technically challenging aspect of this injector. The gun design is based on experience from photoemission gun studies at SLAC [6] and the University of Illinois [7]. The gun electrode structure permits the electric field at the photocathode to be varied between 6 MV/m and 10 MV/m at a constant gun voltage of 500 kV, and can be high voltage processed to approximately 600 kV with the available equipment. The gun is being assembled in the Test Lab where the original CEBAF injector was successfully developed.

Operation of the gun will involve activating a GaAs negative electron affinity (NEA) photocathode in the gun structure proper. This activation requires the application of cesium to the cathode. If this cesium application creates difficulties in maintaining the cathode field strength, we will either fabricate the cathode outside the gun structure, and transfer it to its operating position through a load lock system, or improve the high-field performance of the cathode electrode by appropriate surface treatment.

Ions formed in the immediate vicinity of the photocathode are accelerated back to the cathode, and can cause loss of quantum efficiency through either sputtering or damage to the cathode material. This problem is reduced by minimizing the vacuum pressure in the vicinity of the cathode. The vacuum in the cathode area will be established by non-evaporable getters located in the immediate vicinity of the cathode.

The photocathode will be illuminated by a commercially available CW mode-locked Nd:YLF laser [8]. The fundamental laser light is frequency-doubled to 527 nm in an LBO crystal. The laser provides over 5 W at 527 nm in a mode-locked pulse train at 74.85 MHz. The repetition rate will be halved electro-optically to provide a 37.425 MHz pulse train to the photoemission gun. The 2.5 W of useful laser light will support the required 5 mA average current

for cathodes with quantum efficiencies greater than 1%, assuming losses of no more than 50% in the optical chopping and transport systems. Typical GaAs photoemission cathode quantum efficiencies are an order of magnitude greater than this at 527 nm wavelength, providing a reasonable operating margin.

The two identical solenoids are being fabricated. The design was carried out using POISSON/PARMELA. The spherical aberration from these lenses is negligible. The first solenoid has been placed close to the anode to control the divergent beam out of the gun. It is water-cooled to prevent heat conduction to the gun. Each lens may be operated a factor of 2 stronger than the nominal design requirement.

The 1500 MHz buncher and its associated RF power and control system are under development. The single cell buncher cavity is similar to the fourth cell of the CEBAF capture section, but has a larger inner-bore diameter for the larger beam at this location [9].

The two cryo-unit cavities must provide ~ 10 MV/m at Q_0 of 5×10^9 , both values twice the original CEBAF cavity specification. The cavities are modified to handle the HOM (high order mode) heating, and the increased RF power needed to accelerate the high average current beam. In the injector, each of the four HOM load absorbs 7.5 W of power, sixty times that of CEBAF. This power is dissipated in the 50 K thermal shield rather than the 2 K helium bath. RF shielding is added to the stainless steel bellows and gate valves in the cryo-unit to minimize beam impedance and heating effects. Since the RF power needed in the injector is fourteen times that of CEBAF, the CEBAF style polyethylene warm RF vacuum window is replaced with a ceramic window.

III. PERFORMANCE MODELING

Numerical calculations were needed for: (1) the design of some system components like the solenoids and the injection line magnets; (2) the determination of the optimal element-to-element distances in the system; and (3) the prediction of the system performance. An appropriate space charge algorithm was required for all these tasks.

PARMELA was the skeleton code we used for overall beam dynamics calculations with space charge included consistently from the cathode to the end of the injector. The electric and magnetic field data were provided by other auxiliary codes. The fields in the gun and in the solenoids were calculated using POISSON, which ensured that the field aberrations were included. Mafia was used for calculating the 3-D electromagnetic fields in the SRF cavities [10]. The skew quad effect and steering effect were thus included. The injection line was designed using DIMAD and PARMELA from a large number of iterations between zero-charge and full-charge runs.

A point-by-point space charge algorithm [5] has been used in designing this injector. It is time-consuming but does not assume cylindrical symmetry for the beam. However, for this algorithm, it is crucial to choose properly the particle size factor. This concept simply comes from the fact that when two macroparticles overlap, the charge carried with the source particle must be reduced to account for the shielding effect. A too small particle size factor may result in significant noise in numerically calculating the

space charge fields of a beam [11]. This numerical noise may cause artificial emittance growth, and must be eliminated to obtain a more reliable system layout and a more accurate prediction of the system performance. To size the macroparticles properly, the algorithm was bench-marked against ISIS [12] and MASK [13]. The details of bench-marking will be published elsewhere [14].

The simulated performance of this injector is given in Table 2. As is seen, both transverse and longitudinal emittances are within the requirements by a factor of nearly 2. The simulated rms bunch length of 0.5 ps is within the requirement by a factor of 3. This 0.5 ps is the space-charge-limited minimum bunch length with perfect axial matching [15, 16]. One can trade bunch length for energy spread within at least a factor of 2 by adjusting the degree of axial matching into the bending system, while keeping both the transverse and longitudinal emittances approximately constant.

Table 2 Simulated injector performance

Beam parameters	Sim.	Req.	Units
Momentum	10	10	MeV/c
Charge/bunch	135	135	pC
Tran. norm. rms emit.	4.4	8	π mm mrad
Longitudinal rms emit.	11	20	π keV-deg
Bunch length (rms)	0.5	1.5	ps

The simulated performance in Table 2 was obtained with 8000 macroparticles, and with space charge included through the entire system from the cathode to the end of the injector. The following initial beam parameters were used: gun voltage $V_0 = 500$ kV, DC field gradient at the cathode $E_0 = 10$ MV/m, laser spot size $d_0 = 2$ mm (diameter, $4\sigma_r$) at the cathode, laser pulse length $\Delta t = 90$ ps ($6\sigma_r$); the thermal energy distribution of the electrons emitted at the cathode was assumed to be Gaussian with a mean kinetic energy of $T_e = 0.3$ eV and an rms energy spread of $\sigma_e = 0.1$ eV. System sensitivity studies and alternative operating point studies were conducted as well; see [17] for the details.

IV. EMITTANCE GROWTH

Emittance growth is one of the major concerns with this design. To obtain the best emittance performance for this injector with all the other requirements satisfied, a prescription of minimizing the number of crossovers (very small beam waists) along the system has been adopted. It is obvious that wherever a crossover occurs, more thermal energy will be introduced in the beam due to Coulomb interactions, and beam emittance will increase. The beam phase space distributions may bifurcate after a crossover [13, 18], causing additional emittance growth. With our prescription, the emittance growth from the gun anode to the end of the injector has been minimized to 2π mm mrad for the transverse normalized rms emittance and 4π keV-deg for the longitudinal rms emittance.

In Fig. 2, we show the evolution of various beam properties along the system from the gun anode to the

entrance of the accelerator. The simulations started from the cathode with the initial beam parameters described in the previous section, and continued through the gun, the buncher, the cryounit and the injection beam line to the entrance of the accelerator. With those parameters, the initial transverse normalized rms thermal emittance at the cathode is 0.5π mm mrad. Over the 9-cm distance from the cathode to the gun anode, the emittance increases from 0.5 to 2.3π mm mrad, as shown in Fig. 2, with the beam being accelerated to 500 kV. The beam is strongly divergent before being focussed by the first solenoid located 24 cm from the cathode. In this region, a crossover of electrons trajectory crossing occurs.

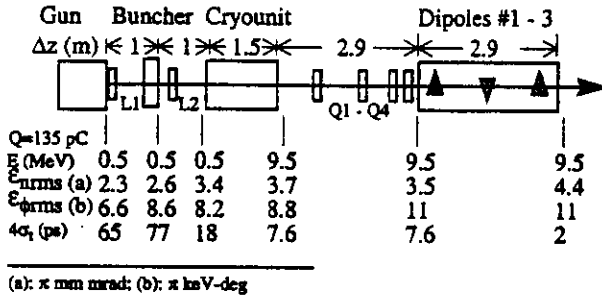


Fig. 2 Beam property evolution along the system

The beam is collimated between the two solenoids. To match the beam into the cryounit, suitable beam conditions must be set up prior to the cryounit. This requires appropriate beam dimensions and correlations in both transverse and longitudinal phase spaces. On the other hand, to avoid emittance growth due to various nonlinear RF field effects, the beam must be three-dimensionally compressed into a small size prior to the cryounit. In this region, the repulsive space charge fields significantly counteract the compression under the external forces from the second solenoid and the buncher. The second crossover occurs between the buncher and the cryounit. As a result, the emittance increases from 2.6 to 3.7π mm mrad with the beam being accelerated to ~ 10 MeV at the exit of the cryounit. As the beam moves through the 3-magnet bending system, the emittance further increases to 4.4π mm mrad at the end of the injector due to space-charge-induced momentum variations [4, 19].

V. A PARAMETRIC COMPARISON

We complete this paper with a parametric comparison of our design with two other DC laser guns in Table 3. The symbols in the first column represent the gun voltage, DC field at the cathode, charge/bunch, diameter of the cathode, diameter of the laser spot on the cathode, rms laser pulse length, repetition rate, and average current. The CEBAF design is characterized by high voltage, short laser pulse length, moderate charge/bunch, and high average current. The SLAC design [20] is characterized by extremely high charge, low voltage, and very long laser pulse length. The design from Ref. [21] is characterized by low average current, moderate pulse length, moderate charge/bunch and low gun voltage.

Table 3 Parametric comparison for DC laser guns

	CEBAF	SLAC	Ref. [21]	Units
V_0	400-500	120	30 - 60	kV
E_0	6 - 10	1.8	15	MV/m
Q	0.07 - 0.2	16	0.02 - 0.6	nC
d_{cath}	25	14	unknown	mm
d_{emit}	2 - 6	14	2	mm
σ_t	15	500	38	ps
f_{rep}	37 MHz	120 Hz	10 Hz	-
I	5 mA	4 μ A	0.2 - 6 nA*	-

* The design average DC current is 5 A in Ref. [21].

We plan to complete the gun performance characterization by the end of this year. This will provide the foundation for us to develop the full injector and also reveal interesting space charge beam physics in our particular parameter regime.

We should note that this design may have other applications besides an FEL driver. One possibility worth studying is use as a source for polarized electrons for a linear collider, though the design would have to be scaled to higher charge.

We wish to thank B. Carlsten and T. Raubenheimer for discussions. This work was supported by the Virginia Center for Innovative Technology and DOE Contract # DE-AC05-84ER40150.

VI. REFERENCES

- [1] C. Sinclair, Nucl. Instr. Meth. A 318 (1992) 410.
- [2] D. Neuffer et al., these proceedings.
- [3] F. Dylla et al., these proceedings.
- [4] H. Liu and D. Neuffer, these proceedings.
- [5] K. McDonald, IEEE Trans. Electron Device ED-35 (1988) 2052.
- [6] C. Sinclair, in *Advanced Accelerator Concepts*, AIP Conf. Proc. No. 156 (Amer. Inst. of Phys., 1987).
- [7] L. Cardman and D. Engwall, private communication.
- [8] S. Benson et al., these proceedings.
- [9] B. Yunn, CEBAF TN# 94-021.
- [10] Z. Li, private communication.
- [11] H. Liu, in *Computational Accelerator Physics*, AIP Conf. Proc. No. 297 (1994).
- [12] M. Jones and B. Carlsten, Proc. 1987 IEEE Part. Acce. Conf., IEEE Catalog No. 87CH2387-9 (1987) 139.
- [13] H. Hanerfeld et al., SLAC-PUB-4916 (1989).
- [14] H. Liu, to be published.
- [15] T. Raubenheimer, Workshop on 4th generation light sources, SSRL, 1993, p.263.
- [16] H. Liu, CEBAF TN # 95-004, 1995.
- [17] FEL Conceptual Design Report, CEBAF, 1995.
- [18] H. Liu et al., Nucl. Instr. Meth. A 358 (1995) 475.
- [19] B. Carlsten and T. Raubenheimer, Phys. Rev. E, 51 (1995) 1453.
- [20] H. Tang et al., Proc. 1993 PAC, p. 3036.
- [21] A. Aleksandrov et al., Phys. Rev. E, 51 (1995) 1449.